MATERIALS SCIENCE / МАТЕРИАЛОВЕДЕНИЕ

UDC 536.425:539.25:539.351
DOI 10.17073/0368-0797-2024-2-185-194

Original article
Оригинальная статья

Formation of the gradient of structural-phase states of high-speed steel during surfacing. Part 2. The role of the Mullins–Sekerka instability in formation of crystallization structures

S. A. Nevskii[1], L. P. Bashchenko[1], V. E. Gromov[1], O. A. Peregudov[2], A. N. Gostevskaya[1], T. V. Volodin[1]

[1] **Siberian State Industrial University** (42 Kirova Str., Novokuznetsk, Kemerovo Region – Kuzbass 654007, Russian Federation)
[2] **Omsk State Technical University** (11 Mira Ave., Omsk 644050, Russian Federation)

nevskiy.sergei@yandex.ru

Abstract. The authors studied the crystallization process of the Fe – W system, which is the basis of heat-resistant high-speed steel used in plasma arc surfacing on the surface of rolls and various cutting tools. The structure of this material consists of two components: cellular and dendritic. Histogram of the structural elements distribution shows the presence of a single maximum. The most probable size takes a value in the range of 10 – 15 μm. The paper considers the morphological instability of crystallization front (the Mullins-Sekerka instability). The model includes the equations of convective thermal conductivity and diffusion. The Stefan conditions for temperature were set at interface of the phases. Linear analysis of this instability is carried out for two cases: when the convective term in the equations of thermal conductivity and diffusion can be neglected; when convection prevails over diffusion processes. In all cases, it was assumed that the value $(1 - k_s)$ was close to zero, which corresponds to a concentration of the alloying element approximately equal to or exceeding the eutectic one, and a short-wave approximation was also used. In the first case, the analytical view of dependence of the wavelength, which accounts for the maximum rate of interface disturbances growth, coincides with generally accepted concepts. In the second case, the value of this wavelength is directly proportional to square root of the interphase boundary velocity. The limits of applicability of these approximations for various mechanisms of crystal growth were determined. In the case of normal growth, both approximations provide an adequate explanation for the formation of structural elements up to 5 μm in size at a crystallization front velocity of about 2 m/s. For the case of growth due to screw dislocations, the wavelength value corresponding to the fastest-growing perturbation mode in the first case coincides with experimental data at a crystallization front velocity of the order of 10^{-7} m/s, whereas in the convective approximation such a coincidence is observed at 10^{-4} m/s. Further development of the model consists in simultaneous consideration of the convective and diffusion components. The results obtained will serve as a material for the research of the Mullins-Sekerka instability for two interface boundaries.

Keywords: Fe – W system, the Mullins–Sekerka morphological instability, equation of thermal conductivity, mobile boundaries of phase transformations

Acknowledgements: The research was supported by the Russian Science Foundation (grant No. 23-19-00186), https://rscf.ru/project/23-19-00186/.

For citation: Nevskii S.A., Bashchenko L.P., Gromov V.E., Peregudov O.A., Gostevskaya A.N., Volodin T.V. Formation of the gradient of structural-phase states of high-speed steel during surfacing. Part 2. The role of the Mullins-Sekerka instability in formation of crystallization structures. *Izvestiya. Ferrous Metallurgy*. 2024;67(2):185–194. https://doi.org/10.17073/0368-0797-2024-2-185-194

Формирование градиента структурно-фазовых состояний быстрорежущей стали при наплавке. Часть 2. Роль неустойчивости Маллинза–Секерки в образовании структур кристаллизации

С. А. Невский[1], Л. П. Бащенко[1], В. Е. Громов[1], О. А. Перегудов[2], А. Н. Гостевская[1], Т. В. Володин[1]

[1] **Сибирский государственный индустриальный университет** (Россия, 654007, Кемеровская обл. – Кузбасс, Новокузнецк, ул. Кирова, 42)
[2] **Омский государственный технический университет** (Россия, 644050, Омск, пр. Мира, 11)

nevskiy.sergei@yandex.ru

Аннотация. Изучен процесс кристаллизации системы Fe – W, которая лежит в основе теплостойкой быстрорежущей стали, применяемой в процессе плазменно-дуговой наплавки на поверхность валков и различных режущих инструментов. Исследования структуры данного материала показали, что структура состоит из двух составляющих: ячеистой и дендритной. Гистограмма распределения структурных элементов показывает наличие одного максимума. Наиболее вероятный размер находится в диапазоне 10 – 15 мкм. В работе рассматривается морфологическая неустойчивость фронта кристаллизации (неустойчивость Маллинза–Секерки). Модель включает в себя уравнения конвективной теплопроводности и диффузии. На границе раздела фаз задавались условия Стефана для температуры. Линейный анализ данной неустойчивости проводится для двух случаев: когда конвективным членом в уравнениях теплопроводности и диффузии можно пренебречь; когда конвекция преобладает над диффузионными процессами. Во всех случаях предполагается, что величина $(1 - k_s)$ близка к нулю, что соответствует концентрации легирующего элемента, примерно равной эвтектической или превышающей ее, а также используется коротковолновое приближение. В первом случае аналитический вид зависимости длины волны, на которую приходится максимум скорости роста возмущений межфазной границы, совпадает с общепринятыми представлениями. Во втором случае значение данной длины волны прямо пропорционально квадратному корню из скорости движения межфазной границы. Определены границы применимости данных приближений для различных механизмов роста кристаллов. В случае нормального роста оба приближения дают адекватное объяснение образованию структурных элементов размерами до 5 мкм при скорости фронта кристаллизации порядка 2 м/с. Для случая роста за счет винтовых дислокаций значение длины волны, соответствующей наиболее быстрорастущей моды возмущений в первом случае, совпадает с экспериментальными данными при скорости фронта кристаллизации порядка 10^{-7} м/с, тогда как в конвективном приближении такое совпадение наблюдается при 10^{-4} м/с. Дальнейшее развитие модели заключается в одновременном учете конвективной и диффузионной составляющих. Полученные результаты послужат материалом для исследования неустойчивости Маллинза–Секерки для двух границ раздела.

Ключевые слова: система железо – вольфрам, морфологическая неустойчивость Маллинза–Секерки, уравнение теплопроводности, подвижные границы фазовых превращений

Благодарности: Исследование выполнено при финансовой поддержке Российского научного фонда (грант № 23-19-00186), https://rscf.ru/project/23-19-00186/).

Для цитирования: Невский С.А., Бащенко Л.П., Громов В.Е., Перегудов О.А., Гостевская А.Н., Володин Т.В. Формирование градиента структурно-фазовых состояний быстрорежущей стали при наплавке. Часть 2. Роль неустойчивости Маллинза–Секерки в образовании структур кристаллизации. *Известия вузов. Черная металлургия*. 2024;67(2):185–194. https://doi.org/10.17073/0368-0797-2024-2-185-194

Introduction

High-speed steels are increasingly used as wear-resistant coating materials, applied by plasma spraying onto the working surfaces of mining and metallurgical equipment subjected to abrasive wear conditions [1]. These steels exhibit high mechanical properties such as hardness and wear resistance. However, the spraying process can lead to the formation of structures that cause cracks and reduce hardness, preventing the full utilization of the high-performance characteristics of high-alloy, heat-resistant alloys [2]. To maintain the high mechanical properties of the resulting coating, additional heat treatments [3] or adjustments to the spraying parameters [4] are necessary. Optimal spraying parameters require an understanding of the material crystallization processes and the associated structural-phase transformations. The formation of specific structures (cellular or dendritic) during the action of concentrated energy fluxes is explained by the morphological instability of the crystallization front, known as Mullins–Sekerka instability [5; 6].

Currently, various authors are studying this instability [7 – 10]. In [7], the instability was examined for binary alloys. Criteria for absolute and relative stability of a spherical crystallization nucleus were formulated for these alloys, and it was demonstrated that as the particle size increases, the initial concentration in the diluted binary melt initially suppresses and then enhances the morphological stability of the particle. The critical concentration at which this effect begins was also determined. The work described in [8] focuses on studying

the influence of an incoming melt flow on the crystallization front of supercooled liquids with a two-phase layer. It was found that the incoming melt flow plays a crucial role in the changes in the parameters of the two-phase layer and its internal structure. The proportion of the solid phase in this layer and its thickness significantly increase, while its permeability and average distance between dendrites decrease with increasing intensity of the incoming melt flow. In [9], the verification of results from linear stability analysis using the phase field method in multi-component melts with a planar solidification front demonstrated that, despite using a unified set of equations for linear stability analysis under various solidification conditions, theoretical differences between directional and isothermal solidification should be noted. Specifically, in the case of directional solidification, if considering the steady-state solution of the planar problem, the equilibrium compositions at the interface are invariant with respect to the choice of the diffusion coefficient matrix, thus allowing the change in concentration gradients ahead of the interface, which affect instability behavior, to be easily determined since the interface velocity is known [9]. Conversely, in isothermal solidification, the planar problem does not have a steady-state solution characterized by a constant system velocity. The growth rate of the interface and the equilibrium compositions depend on the choice of the diffusion coefficient matrix as well as the alloy composition. These characteristics of phase transition affect the growth of morphological perturbations and thus influence the choice of length scales of the microstructure. In [10], similar investigations were conducted on a particle with spherical geometry, taking into account non-stationary terms in the diffusion equations and a complete representation of the diffusion coefficient matrix. This allowed the establishment that stability criteria are not reduced to low velocities as previously thought [11]. The stability of the growing sphere can be considered at high perturbation growth rates, which correspond to high supersaturation. The results clearly show that the threshold values for the destabilization of the growing sphere interface strongly depend on the growth rate. It was also found that the degree of spherical harmonics at which stability is not maintained increases with increasing growth rate. The role of surface tension in the melt is not sufficiently addressed in the presented works [7 – 11], while it can significantly shift the values of the wavelength corresponding to the maximum mode of perturbations [12; 13]. In [12], the dependence of this wavelength on surface tension and crystal growth mechanism is established. It is shown that for most binary compositions considered by the author, the growth mechanism occurs through screw dislocations, and the dependence of λ on $V^{-1/2}$ is practically linear and coincides with experimental data. Surface tension, according to the data from [13], has a significant influence on the kinetic coefficient in the growth model through screw dislocations. Thus, when constructing mathematical models of crystallization of materials under plasma exposure and formulating stability criteria for the interface between the melt and crystal, in addition to concentration supercooling, it is necessary to take into account the role of surface tension and crystal growth mechanisms. As indicated in [14], the instability of Mullins–Sekerka should be studied in several stages: *1* – determine the nature of perturbations of the interface and assess the influence of its curvature on the liquidus temperature; *2* – calculate the temperature and concentration fields in the solid and liquid phases; *3* – find the dependencies of the growth rate of perturbations from conditions at the phase transition boundary. In this study, attention is given to the first and third stages of research, assuming a cylindrical shape of the crystallization front. To verify the obtained results, investigations of the structure of coatings made of high-speed steels after surfacing were conducted using scanning electron microscopy.

Materials and methods

Plasma coating of high-speed steel R18Yu was performed in reverse polarity within a nitrogen protective and alloying environment using non-conductive additive powder wire, as established in [15]. The chemical composition of the steel (wt. %) includes C 0.87; Cr 4.41; W 17.00; Mo 0.10; V 1.50; Ti 0.35; Al 1.15; N 0.06. This composition ensured optimal conditions for wetting the surface of the product with the deposited metal and defect-free formation of the deposited layer. Samples were taken from the upper parts of the deposited layer and subsequently sectioned on an electric spark cutting machine using kerosene for metallographic studies. The samples were then mechanically leveled using fine emery paper and diamond paste, followed by etching of the deformed layer and leveling by an electrolytic method. Studies were conducted using a KYKY-EM6900 scanning electron microscope with a thermionic tungsten cathode equipped with a microprobe attachment. The operating parameters were an accelerating voltage of 20 kV, an emission current of 150 μA, and a filament saturation point of 2.4 A. The working distance between the sample and the objective lens was set at 15 mm. The sizes of the structural elements were determined using the random sectioning method [16].

Results of the experiment

Fig. 1 illustrates the microstructure of the surface layer of the plasma-coated high-speed steel, revealing two morphological components: cellular and dendritic. The grain sizes range from 3 to 45 μm, with the most common sizes between 10 to 15 μm, (Fig. 1, *b*).

The analysis of the histogram (Fig. 1, *b*) highlights that the instability of the crystallization front exhibits a single peak, corresponding to the wavelength that matches the most probable grain size. The presence of two distinct

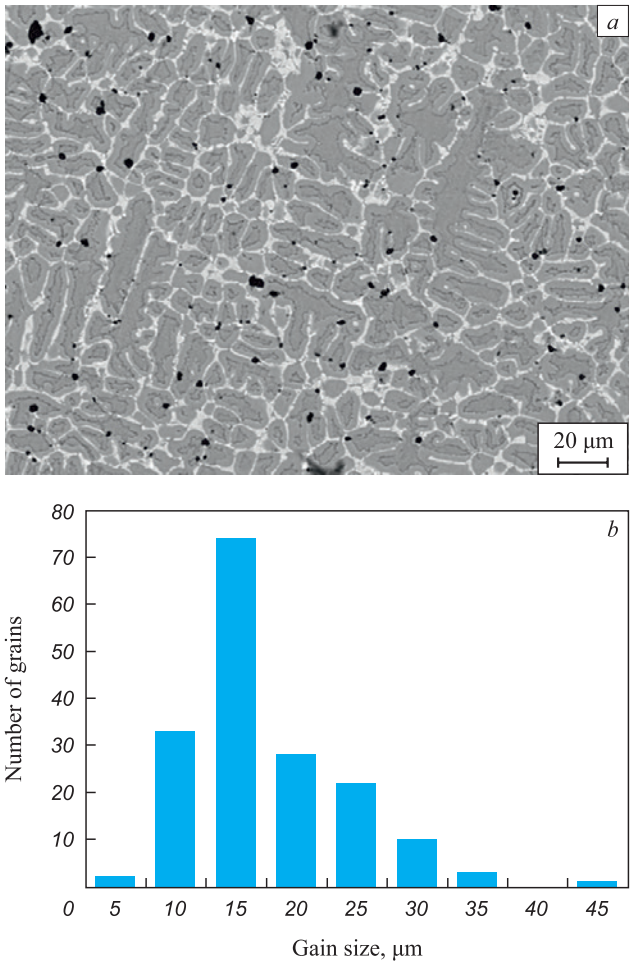

Fig. 1. Microstructure of high–speed steel coating after surfacing (*a*) (electron microscopic image) and histogram of grain size distribution (*b*)

Рис. 1. Микроструктура покрытия из быстрорежущей стали после наплавки (*a*) (электронно-микроскопическое изображение) и гистограмма распределения зерен по размеру (*b*)

morphological components indicates two types of instabilities: “soft”, associated with the cellular structure, and “hard” linked to the dendritic structure.

Formulation of the problem

Let’s examine the stability of the cylindrical crystallization front concerning small harmonic disturbances (Fig. 2).

For the sake of further calculations’ convenience, we introduce the following dimensionless variables, as in [12]:

$$T_l = \frac{T_{lr}}{T_0},\ T_s = \frac{T_{sr}}{T_0},\ C_l = \frac{C_{lr}}{C_0},\ r = \frac{r_r}{a},\ z = \frac{z_r}{a},$$

$$t = \frac{\chi_0}{a^2} t_r,\ D_l = \frac{D_{lr}}{\chi_0},\ \chi_l = \frac{\chi_{lr}}{\chi_0},\ \chi_s = \frac{\chi_{sr}}{\chi_0},$$

where T_{lr}, T_{sr}, C_{lr}, r_r, z_r, D_{lr}, χ_{lr}, χ_{sr} are the dimensional temperatures of the liquid and solid phases, impurity concentrations in the liquid phase, radial and longitudinal coordinates, diffusion coefficient of the impurity in the liquid, thermal diffusivity of the liquid and solid phases, respectively; T_0 is the phase transition temperature (assumed equal to the liquidus temperature); C_0 is the initial impurity concentration, a is the initial radius of the cylindrical nucleus (~1 μm); χ_0 is the characteristic value of the thermal diffusivity coefficient (~10^{-5} m^2/s).

Let us express the latent heat of phase transition ΔH in dimensionless form $\varepsilon = \dfrac{\Delta H}{c_0 T_0}$ (where c_0 is the heat capacity of the substance under study at the phase transition temperature). We will now formulate the equations of thermal conductivity and diffusion in dimensionless form for the solid and liquid phases:

$$\begin{aligned}
&\frac{\partial T_l}{\partial t} - V\frac{\partial T_l}{\partial r} = \chi_l\left(\frac{\partial^2 T_l}{\partial r^2} + \frac{1}{r}\frac{\partial T_l}{\partial r} + \frac{\partial^2 T_l}{\partial z^2}\right);\\
&\frac{\partial T_s}{\partial t} - V\frac{\partial T_s}{\partial r} = \chi_s\left(\frac{\partial^2 T_s}{\partial r^2} + \frac{1}{r}\frac{\partial T_s}{\partial r} + \frac{\partial^2 T_s}{\partial z^2}\right);\\
&\frac{\partial C_l}{\partial t} - V\frac{\partial C_l}{\partial r} = D_l\left(\frac{\partial^2 C_l}{\partial r^2} + \frac{1}{r}\frac{\partial C_l}{\partial r} + \frac{\partial^2 C_l}{\partial z^2}\right).
\end{aligned} \qquad (1)$$

Boundary conditions:

$$\left.\begin{aligned}
&\chi_s\frac{\partial T_s}{\partial r} - \chi_l\frac{\partial T_l}{\partial r} = \varepsilon V;\\
&D_l\frac{\partial C_l}{\partial r} = (1-k_s)C_l V;\\
&T_l = T_s;\ V = V(T, C);
\end{aligned}\right\} \quad \text{at} \quad r = a + \xi(r, z); \qquad (2)$$

$$C_l = 1;\ T_l = T_{00};\ r \to \infty.$$

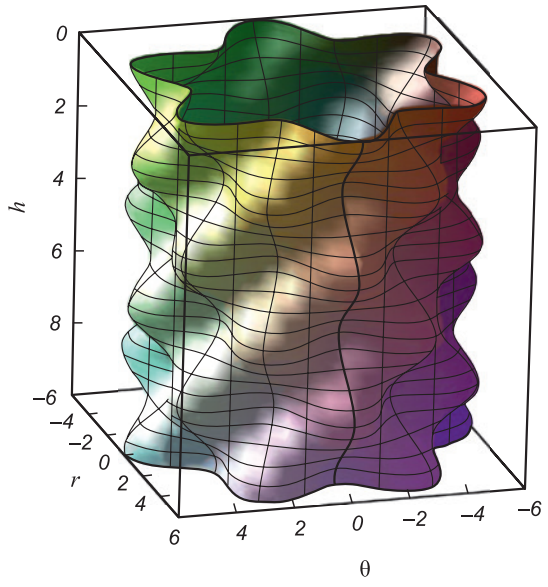

Fig. 2. Geometry of the problem of occurrence of cylindrical crystallization front instability

Рис. 2. Геометрия задачи о возникновении неустойчивости цилиндрического фронта кристаллизации

To analyze the stability of the crystallization front, we express solution (1) as a sum of stationary and disturbed components:

$$\begin{gathered} T_l = T_{0l}(r) + T_{l1}(r, z, t); \\ T_s = T_{0s}(r) + T_{s1}(r, z, t); \\ C_l = C_{0l}(r) + C_{l1}(r, z, t); \\ V = V_s + V_1(r, z, t). \end{gathered} \tag{3}$$

For the stationary component, we have:

$$\begin{gathered} \frac{\partial^2 T_{0l}}{\partial r^2} + \left(\frac{1}{r} + \frac{V_s}{\chi_1}\right)\frac{\partial T_{0l}}{\partial r} = 0; \\ \frac{\partial^2 T_{0s}}{\partial r^2} + \left(\frac{1}{r} + \frac{V_s}{\chi_2}\right)\frac{\partial T_{0s}}{\partial r} = 0; \\ \frac{\partial^2 C_{0l}}{\partial r^2} + \left(\frac{1}{r} + \frac{V_s}{D}\right)\frac{\partial C_{0l}}{\partial r} = 0. \end{gathered} \tag{4}$$

Considering Eq. (3), the boundary conditions for Eq. (4) will be as follows:

$$\left.\begin{gathered} T_{0l} = T_{0s}; \\ \chi_s \frac{\partial T_{0s}}{\partial r} - \chi_l \frac{\partial T_{0l}}{\partial r} = \varepsilon V_s; \\ D_l \frac{\partial C_{0l}}{\partial r} = (1 - k_s) C_{0l} V_s; \\ \chi_s \frac{\partial T_{0s}}{\partial r} = I_0; \end{gathered}\right\} \text{ at } r = a; \tag{5}$$

$$\begin{gathered} C_{0l} = 1,\ T_l = T_{00},\ r \to \infty; \\ T_{0s} = T_0,\ r = r_0. \end{gathered}$$

The interface perturbation equations will be as follows:

$$\begin{gathered} \frac{\partial T_{l1}}{\partial t} - V_s \frac{\partial T_l}{\partial r} - V_1 G_l = \chi_l \left(\frac{\partial^2 T_{l1}}{\partial r^2} + \frac{1}{r}\frac{\partial T_{l1}}{\partial r} + \frac{\partial^2 T_{l1}}{\partial z^2}\right); \\ \frac{\partial T_{s1}}{\partial t} - V_s \frac{\partial T_{s1}}{\partial r} - V_1 G_s = \chi_s \left(\frac{\partial^2 T_{s1}}{\partial r^2} + \frac{1}{r}\frac{\partial T_{s1}}{\partial r} + \frac{\partial^2 T_{s1}}{\partial z^2}\right); \\ \frac{\partial C_{l1}}{\partial t} - V_s \frac{\partial C_{l1}}{\partial r} - V_1 G_c = D_l \left(\frac{\partial^2 C_{l1}}{\partial r^2} + \frac{1}{r}\frac{\partial C_{l1}}{\partial r} + \frac{\partial^2 C_{l1}}{\partial z^2}\right). \end{gathered} \tag{6}$$

Accordingly, boundary conditions (2) will be as follows:

$$\left.\begin{gathered} T_{l1} = T_{s1}; \\ \chi_s \frac{\partial T_{s1}}{\partial r} - \chi_l \frac{\partial T_{l1}}{\partial r} = \varepsilon V_s; \\ D_l \frac{\partial C_{l1}}{\partial r} = (1 - k_s)(V_s C_{l1} + C_{0l} V_1); \end{gathered}\right\} \text{ at } r = a; \tag{7}$$

$$\begin{gathered} C_{l1} = 0;\ T_{l1} = 0;\ r \to \infty; \\ T_{s1} = 0;\ r \to 0. \end{gathered}$$

Analyzing linear stability requires knowledge of the analytical form of the unperturbed temperature gradients included in equation (6). To obtain them, we need to solve the boundary value problem (4), (5). Let's present the solutions to this problem in the form:

$$\begin{gathered} T_{0l} = T_{00} + \left(\frac{T_0 - T_{00}}{Ei\left(\frac{V_s a}{\chi_l}\right)} + \right. \\ \left. + \frac{\frac{I_0 a}{\chi_s} \exp\left(\frac{V_s a}{\chi_s}\right)\left[Ei\left(\frac{V_s r_0}{\chi_s}\right) - Ei\left(\frac{V_s a}{\chi_s}\right)\right]}{Ei\left(\frac{V_s a}{\chi_l}\right)} \right) Ei\left(\frac{V_s}{\chi_l} r\right); \\ T_{0s} = T_0 + \frac{I_0 a}{\chi_s} \exp\left(\frac{V_s a}{\chi_s}\right)\left[Ei\left(\frac{V_s r_0}{\chi_s}\right) - Ei\left(\frac{V_s r}{\chi_s}\right)\right]; \\ C_{0l} = 1 + \frac{V_s a (1 - k_s) Ei\left(\frac{V_s r}{D_l}\right)}{V_s a (k_s - 1) Ei\left(\frac{V_s a}{D_l}\right) + D_l \exp\left(-\frac{V_s a}{D_l}\right)}. \end{gathered} \tag{8}$$

Let us proceed to solve the boundary value problem (6) and (7) for perturbations of temperature, concentration, and velocity of the crystallization front. We will seek its solution in the following form:

$$\begin{gathered} T_{l1}(r, z, t) = T_{m1}(r) \exp(\omega t + kz); \\ T_{s1}(r, z, t) = T_{m2}(r) \exp(\omega t + kz); \\ C_{l1}(r, z, t) = C_{m1}(r) \exp(\omega t + kz); \\ V_1 = V_m(r) \exp(\omega t + kz), \end{gathered} \tag{9}$$

where $\omega = \omega_1 + i\omega_2$; $k = k_1 + ik_2$.

Then, equations (6) will take the form:

$$\begin{gathered} \frac{d^2 T_{m1}}{dr^2} + \left(\frac{1}{r} + \frac{V_s}{\chi_l}\right)\frac{dT_{m1}}{dr} + \frac{\chi_l k^2 - \omega}{\chi_l} T_{m1} = -\frac{V_m}{\chi_l} G_l; \\ \frac{d^2 T_{m2}}{dr^2} + \left(\frac{1}{r} + \frac{V_s}{\chi_l}\right)\frac{dT_{m2}}{dr} + \frac{\chi_s k^2 - \omega}{\chi_s} T_{m2} = -\frac{V_m}{\chi_s} G_s; \\ \frac{d^2 C_m}{dr^2} + \left(\frac{1}{r} + \frac{V_s}{D_l}\right)\frac{dC_m}{dr} + \frac{D_l k^2 - \omega}{D_l} C_m = -\frac{V_m}{D_l} G_c. \end{gathered} \tag{10}$$

Accordingly, the boundary conditions (7) take the form (where the prime denotes the derivative with respect to the radial coordinate):

$$\begin{gathered} T_{m1}(a) = T_{m2}(a); \\ \chi_s T_{m2}(a)' - \chi_l T_{m1}(a)' = \varepsilon V_m(a); \\ D_l C_m(a)' = (k_s - 1)\left[V_s C_m(a) + C_{0l} V_m(a)\right]; \\ C_m = 0;\ T_{m1} = 0;\ r \to \infty;\ T_{m2} = 0;\ r \to 0. \end{gathered} \tag{11}$$

As in equation [1], the amplitude of interphase boundary velocity disturbances as a function of maximum temperature and concentration disturbances is as follows:

$$V_m(a) = \theta T_{m1}(a) + \gamma C_m(a), \qquad (12)$$

where $\theta = \frac{\partial V}{\partial T}$; $\gamma = \frac{\partial V}{\partial C}$.

Dispersion equation of perturbations of phase transition boundary

Equations (10) are degenerate inhomogeneous hypergeometric equations whose solutions are Kummer functions. Obtaining and analyzing the dispersion equation, which includes these functions, is a complex and nontrivial task. Therefore, we will limit ourselves to considering special cases. In the first case, we neglect the convective term in equation (1). Then, stationary solutions are as follows:

$$T_{0l} = T_{00} + \frac{a\ln\left(\frac{r}{b_1}\right)(I_0 - \varepsilon V_s)}{\chi_l};$$
$$T_{0s} = T_0 + \frac{a\ln\left(\frac{r}{b}\right)I_0}{\chi_s}; \qquad (13)$$
$$C_{0l} = 1 + \frac{(k_s - 1)V_s a\ln\left(\frac{r}{b_1}\right)}{(1-k_s)aV_s\ln\left(\frac{r}{b_1}\right) + D_l}.$$

Accordingly, equation (10) are as follows:

$$\frac{d^2T_{m1}}{dr^2} + \frac{1}{r}\frac{dT_{m1}}{dr} - S_1^2T_{m1} = 0;$$
$$\frac{d^2T_{m2}}{dr^2} + \frac{1}{r}\frac{dT_{m2}}{dr} - S_2^2T_{m2} = 0; \qquad (14)$$
$$\frac{d^2C_m}{dr^2} + \frac{1}{r}\frac{dC_m}{dr} - S_3^2C_m = 0,$$

where $S_1^2 = \frac{\omega}{\chi_l} - k^2$; $S_2^2 = \frac{\omega}{\chi_s} - k^2$; $S_3^2 = \frac{\omega}{D_l} - k^2$.

Solutions (14) are as follows:

$$T_{m1} = A_1I_0(S_1r) + A_2K_0(S_1r);$$
$$T_{m2} = A_3I_0(S_2r) + A_4K_0(S_2r); \qquad (15)$$
$$C_m = A_5I_0(S_3r) + A_6K_0(S_3r).$$

Substituting equations (15) into boundary conditions (11) and subsequent transformations, taking into account equation (12), lead to the following dispersion equation:

$$\left(\frac{K_0(S_1a)I_1(S_2a)S_2}{I_0(S_2a)}\chi_2 + \chi_1K_1(S_1a)S_1 - \varepsilon\theta K_0(S_1a)\right)\times$$
$$\times\left[(1-k_s)K_0(S_3a)(C_{0l}\gamma + V_s) - D_lK_1(S_3a)S_3\right] +$$
$$+(1-k_s)\varepsilon\gamma C_{0l}K_0(S_3a)K_0(S_1a)\theta = 0. \qquad (16)$$

At an impurity concentration approximately equal to the eutectic, the value $(1 - k_s)$ is close to zero, therefore, these terms in dependence (16) can be neglected. As a result, we have:

$$\frac{I_1(S_2a)}{I_0(S_2a)}S_2\chi_2 + \frac{K_1(S_1a)}{K_0(S_1a)}S_1\chi_1 - \varepsilon\theta = 0. \qquad (17)$$

The value of θ, as in [1], is considered equal to $\frac{\Lambda\omega}{\Lambda\Gamma k^2 - \omega}$ (where $\Lambda = \frac{\partial V}{\partial \Delta T}$ is a coefficient depending on the crystal growth mechanism; $\Gamma = \alpha\Gamma_r$; Γ_r is the ratio of the product of surface tension and phase transition temperature to the volumetric latent energy of phase transformation; $\alpha = 1/(aT_0)$).

In the case of short waves, where $S_{1,2} \gg 1$, the approximate values of the Bessel functions can be represented as

$$I_0(S_2a) \approx I_1(S_2a) \approx \frac{\exp(S_2a)}{\sqrt{2\pi S_2a}}$$

and

$$K_0(S_1a) \approx K_1(S_1a) \approx \frac{\pi\exp(-S_1a)}{\sqrt{2\pi S_1a}}.$$

Then, equation (17) is as follows

$$S_2\chi_2 + S_1\chi_1 - \varepsilon\theta = 0. \qquad (18)$$

We assume that $k_1 = 0$ and $\omega_2 = 0$, then $S_1 = \sqrt{k_2^2 + \frac{\omega_1}{\chi_l}}$, $S_2 = \sqrt{k_2^2 + \frac{\omega_1}{\chi_s}}$. Let us substitute as follows: $\omega_1 = \frac{\delta V_s^2}{D_l}$, $k_2^2 = \frac{V_s^2}{D_l^2}Y$. Then, $S_1 = \frac{V_s}{D_l}\sqrt{Y + \frac{\delta D_l}{\chi_l}}$, $S_2 = \frac{V_s}{D_l}\sqrt{Y + \frac{\delta D_l}{\chi_s}}$. Provided that $Y \gg \frac{\delta D_l}{\chi_s}$ and at $\delta \sim Y$ the maximum growth rate will be observed at the wavelength

$$\lambda = \frac{2\pi(\chi_l + \chi_s)}{\varepsilon\Lambda}(1 + \Lambda\Gamma). \qquad (19)$$

Thus, it can be concluded that equation (19) completely coincides with the dependency obtained in [12]. This allows us to infer that in the short-wave approximation, considering only diffusion terms, the problem of finding the wavelength at which the growth rate maximum occurs simplifies for cylindrical geometry to a problem on a plane.

In the second case, we neglect the diffusion term in equation (6). Then the equation takes the form:

$$\begin{aligned}
&\frac{\partial T_{l1}}{\partial t} - V_s \frac{\partial T_l}{\partial r} - V_1 G_l = 0;\\
&\frac{\partial T_{s1}}{\partial t} - V_s \frac{\partial T_{s1}}{\partial r} - V_1 G_s = 0;\\
&\frac{\partial C_{l1}}{\partial t} - V_s \frac{\partial C_{l1}}{\partial r} - V_1 G_c = 0.
\end{aligned} \tag{20}$$

Substitution of solutions (22) into boundary conditions (11), subsequent transformations taking into account (12) lead to the following dispersion equation:

$$\begin{aligned}
&\frac{dT_{m1}}{dr} - \frac{\omega}{V_s} T_{m1} = 0;\ \frac{dT_{m2}}{dr} - \frac{\omega}{V_s} T_{m2} = 0;\\
&\frac{dC_m}{dr} - \frac{\omega}{V_s} C_m = 0.
\end{aligned} \tag{21}$$

The solutions are as follows:

$$\begin{aligned}
&T_{m1} = A_1 \exp\left(\frac{\omega r}{V_s}\right);\ T_{m2} = A_2 \exp\left(\frac{\omega r}{V_s}\right);\\
&C_m = A_3 \exp\left(\frac{\omega r}{V_s}\right).
\end{aligned} \tag{22}$$

Substituting solutions (22) into boundary conditions (11), subsequent transformations taking into account (12), lead to the following dispersion equation:

$$\begin{aligned}
&\left(\frac{(\chi_s - \chi_l)\omega}{V_s} - \varepsilon\theta\right)\left(\frac{D_l \omega}{V_s} - (k_s - 1)(V_s + C_0\gamma)\right) -\\
&-\gamma\varepsilon(k_s - 1)C_0\theta = 0.
\end{aligned} \tag{23}$$

Also, as in the previous case, in equation (23) we neglect the terms that contain $(k_s - 1)$. As a result, we get

$$\frac{(\chi_s - \chi_l)\omega}{V_s} - \varepsilon\theta = 0. \tag{24}$$

The maximum growth rate of disturbances is observed at a wavelength

$$\lambda = \frac{2\pi\sqrt{\varepsilon V_s \Lambda(\chi_s - \chi_l)(1 + \Gamma\Lambda)}}{\varepsilon\Lambda V_s}. \tag{25}$$

During normal crystal growth, the crystallization front velocity is directly proportional to the degree of undercooling $V_s = h\Delta T$ [12; 13] (where h is the proportionality coefficient; ΔT is undercooling). Then $\Lambda = h$. According to model [13], the dimensional value of the coefficient h is determined as

$$h_r = \frac{\beta D_{lr} \Delta H M}{\Delta l R T_{rL}^2}, \tag{26}$$

where M is the molar weight; R is the universal gas constant; Δl is the disturbance amplitude of the interface (approximately 0.1 nm); T_{rL} is the liquidus temperature; β is the coefficient that accounts for the difference between the mean free path of molecules in the liquid phase and the period of the crystalline lattice, as well as the symmetry of the molecules (for symmetric molecules β ~ 10).

According to the data from the Table in equation (26), it follows that with an initial nucleus size of 1 μm, the value of the coefficient h_r is 0.558 m/(s·K).

The transition to dimensional variables in equation (19) gives

$$\lambda_r = \frac{2\pi(\chi_{lr} + \chi_{sr})}{\frac{\Delta H}{c_0} h_r}\left(1 + h_r \frac{\Gamma_r}{\chi_0}\right). \tag{27}$$

The crystallization front velocity is determined based on the data from reference [14] as follows $V_{sr} = \frac{\Delta a}{\Delta t}$, knowing the undercooling, we determine h_r. Reference [14] indicates that $\Delta a = 10^{-8}$ m, and $\Delta\tau = 4.4118$ ns, then $V_{sr} = 2.27$ m/s and $h_r = 0.757$ m/(a·K) for an undercooling of 3 K. The coefficient Γ_r is determined as $\Gamma_r = \frac{\gamma T_{Lr}}{\Delta H \rho} =$ $= 1.71 \cdot 10^{-6}$ K·m. Calculation according to equation (27) shows that in the case when h_r is 0.558 m/(s·K), $\lambda = 0.382$ μm. With $h_r = 0.757$ m/(s·K), calculation according to equation (27) leads to $\lambda = 0.291$ μm. Calculation based on equation (25) shows that for $h_r = 0.558$ m/(s·K), $\lambda = 0.324$ μm, and for $h_r = 0.757$ m/(s·K), $\lambda = 0.242$ μm. Comparison of the obtained results with the grain sizes in Fig. 1, *b* shows that both convective and diffusive approximations provide an explanation for grain size formation through the mechanism of normal growth

Characteristics of the Fe–W system

Характеристики системы железо – вольфрам

Properties of material	Symbol	Value
Liquidus point, K	T_{Lr}	1806
Specific heat of melting, kJ/kg	ΔH	270
Density, kg/m^3	ρ	6980
Diffusion coefficient, m^2/s	D_r	10^{-8}
Specific heat capacity, J/(kg·K)	c_0	611
Thermal diffusivity of the liquid phase, m^2/s	χ_1	$6.8 \cdot 10^{-6}$
Thermal diffusivity of the solid phase, m^2/s	χ_2	$6.9 \cdot 10^{-6}$
Surface tension, N/m	γ	1.788

up to 5 μm, although the maximum is found at sizes of 10 – 15 μm. This suggests that under these conditions, the normal growth model is not adequate. Let us consider the growth mechanism through screw dislocations. The crystallization front velocity in this case is directly proportional to the square of the undercooling. In this case $\Lambda = 2\sqrt{hV_s}$ [12], equation (19) will take the form:

$$\lambda = \frac{\pi(\chi_l + \chi_s)}{\varepsilon\sqrt{hV_s}}\left(1 + 2\sqrt{hV_s}\Gamma\right). \quad (28)$$

Returning to the dimensional variables in equation (28), we obtain

$$\lambda_r = \frac{\pi(\chi_{lr} + \chi_{sr})}{\frac{\Delta H}{c_0}\sqrt{h_r V_{sr}}}\left(1 + 2\sqrt{h_r V_{sr}}\frac{\Gamma_r}{\chi_0}\right). \quad (29)$$

For the growth mechanism through screw dislocations, the value of the kinetic coefficient h_r is determined as

$$h_r = \frac{\beta\left(1 + 2g^{1/2}\right)D_{lr}(\Delta HM)^2}{4\pi g R T_{rL}^3 \gamma V_m}, \quad (30)$$

where $g = 2\pi^4 n^3 \exp\left(-\frac{\pi^2 n}{2}\right)$; n is the number of molecular layers [16]; V_m is the molar volume.

For metallic materials, when $n \sim 6$, $g \sim 5.99 \cdot 10^{-9}$. The value of the kinetic coefficient h_r, calculated from the table data for the growth model through screw dislocations, is 433 m/(s·K^2). The value of the wavelength, calculated using equation (30) with this value of h_r and a crystallization front velocity of about 10^{-7} m/s, is 14.8 μm, which coincides with the most probable grain size values in Fig. 1, *b*. In the convective approximation, calculation using equation (25) shows that the wavelength takes values of the order of 10^4 μm. This suggests a predominance of diffusion processes at these crystallization front velocities. When the crystallization velocity is increased by three orders of magnitude, λ = 14.9 μm, which matches the experimental data. Thus, the convective approximation is significant for crystallization velocities greater than 10^{-4} m/s. Based on the above, it can be concluded that the Mullins–Sekerka instability provides an adequate explanation for the formation of cellular structures with sizes of about 10 μm at $V_s < 1$ m/s and undercooling degrees of about ~10^{-5} K. When a volumetric heat source acts on the surface of the irradiated material, as shown in [17; 18], obtained using the phase-field method, the transformation front velocity can range from 10^{-7} to 10^3 m/s, depending on the power density of the source and the characteristics of the medium. These works [19; 20] indicate that the action of this source leads to the occurrence of large temperature gradients in the surface layers of the material and, as a result, to the emergence of thermocapillary effects. This allows us to conclude that to build a crystallization model, in addition to the Mullins–Sekerka morphological instability, it is necessary to take into account other instabilities (thermocapillary and concentration-capillary) that occur in the molten material. Analysis of the dispersion equations obtained in [21; 22] for these instabilities showed that for the Fe – W system under consideration, the wavelength corresponding to the maximum disturbances is 12 μm, which also coincides with experimental data.

Conclusions

The theoretical study conducted on the formation of cellular structures during the crystallization process of the iron-tungsten system, by analyzing the dispersion equation characterizing the morphological instability of the crystallization front (the Mullins–Sekerka instability), revealed that the mechanism of normal crystal growth provides an adequate explanation for the formation of cells with sizes up to 5 μm when the convective term can be neglected. Additionally, the growth mechanism through screw dislocations leads to λ = 14.8 μm, coinciding with experimental data under the condition that the crystallization front velocity is less than 1 m/s and the undercooling degree is about ~10^{-5} K. Further development of the presented model involves incorporating thermocapillary and concentration-capillary effects.

References / Список литературы

1. Mozgovoi I.V., Shneider E.A. High-Speed Steel Surfacing. Omsk: izd. OmGTU; 2016:200. (In Russ.).
Мозговой И.В., Шнейдер Е.А. Наплавка быстрорежущей стали. Омск: изд. ОмГТУ; 2016:271.
2. Wang Yu., Mao B., Chu S., Chen S., Xing H., Zhao H., Wang S., Wang Y., Zhang J., Sun B. Advanced manufacturing of high-speed steels: A critical review of the process design, microstructural evolution, and engineering performance. *Journal of Materials Research and Technology*. 2023;24:8198–8240. https://doi.org/10.1016/j.jmrt.2023.04.269
3. Lavrentiev A.Yu., Dozhdelev A.M. Improvement of the structure of the zone of thermal influence of a deposited bimetallic tool. *Scientific and Technical Bulletin of St. Petersburg State University. Natural and Engineering Sciences*. 2017;23(3):118–126. (In Russ.). https://doi.org/10.18721/JEST.230311
Лаврентьев А.Ю., Дожделев А.М. Совершенствование структуры зоны термического влияния наплавленного биметаллического инструмента. *Научно-технические ведомости СПбПУ. Естественные и инженерные науки*. 2017;23(3):118–126. https://doi.org/10.18721/JEST.230311
4. Cao H.T., Dong X.P., Pan Z., Wu X.W., Huang Q.W., Pei Y.T. Surface alloying of high-vanadium high-speed steel on ductile iron using plasma transferred arc technique: Microstructure and wear properties. *Materials & Design*. 2016;100:223–234. https://doi.org/10.1016/j.matdes.2016.03.114

5. Sekerka R.F. Morphological stability. *Journal of Crystal Growth*. 1968;3-4:71–81. https://doi.org/10.1016/0022-0248(68)90102-4
6. Merchant G.J., Davis S.H. Morphological instability in rapid directional solidification. *Acta Metallurgica et Materialia*. 1990;38(12):2683–2693. https://doi.org/10.1016/0956-7151(90)90282-L
7. Chen M.W., Wang Z.D. The evolution and morphological stability of a particle in a binary alloy melt. *Journal of Crystal Growth*. 2023;607:127113. https://doi.org/10.1016/j.jcrysgro.2023.127113
8. Alexandrov D.V., Toropova L.V. The role of incoming flow on crystallization of undercooled liquids with a two-phase layer. *Scientific Reports*. 2022;12:17857. https://doi.org/10.1038/s41598-022-22786-w
9. Lahiri A., Choudhury A. Theoretical and numerical investigation of diffusive instabilities in multicomponent alloys. *Journal of Crystal Growth*. 2017;459:1–12. http://dx.doi.org/10.1016/j.jcrysgro.2016.11.046
10. Guillemot G., Gandin C.-A. Morphological stability of spherical particles – Extension of the Mullins-Sekerka criteria to multi-component alloys under a non-stationary diffusive regime. *Acta Materialia*. 2021;205:116539. https://doi.org/10.1016/j.actamat.2020.116539
11. Colin J., Voorhees P.W. Morphological instability of a solid sphere of dilute ternary alloy growing by diffusion from its melt. *Journal of Crystal Growth*. 2016;448:17–20. https://doi.org/10.1016/j.jcrysgro.2016.03.041
12. Gus'kov A.P. Dependence of structure period on interphase boundary velocity during eutectics crystallization. *Zhurnal tekhnicheskoi fiziki*. 2003;73(5):46–52. (In Russ.).

    Гуськов А.П. Зависимость периода структуры от скорости межфазной границы при кристаллизации эвтектик. *Журнал технической физики*. 2003;73(5):46-52.
13. Gus'kov A.P., Orlov A.D. Dependence of period of macrostructures on kinetic parameters under directed crystallization. *Computational Materials Science*. 2002;24(1-2):93–98. https://doi.org/10.1016/S0927-0256(02)00169-6
14. Nevskii S.A., Bashchenko L.P., Peregudov O.A. Formation of the gradient of structural-phase states of high-speed steel during surfacing. Part 1. Solving the Stefan problem with two movable boundaries. *Izvestiya. Ferrous Metallurgy*. 2023;66(5):587–593. https://doi.org/10.17073/0368-0797-2023-5-587-593

    Невский С.А., Бащенко Л.П., Перегудов О.А. Формирование градиента структурно-фазовых состояний быстрорежущей стали при наплавке. Часть 1. Решение задачи Стефана с двумя подвижными границами. *Известия вузов. Черная металлургия*. 2023;66(5):587–593. https://doi.org/10.17073/0368-0797-2023-5-587-593
15. Malushin N.N., Romanov D.A., Kovalev A.P., Osetkovskii V.L., Bashchenko L.P. Structural-phase state of a heat-resistant alloy of high hardness formed by plasma surfacing in nitrogen medium and high-temperature tempering. *Izvestiya vuzov. Fizika*. 2019;62(10(742)):106–111. (In Russ.).

    Малушин Н.Н., Романов Д.А., Ковалев А.П., Осетковский В.Л., Бащенко Л.П. Структурно-фазовое состояние теплостойкого сплава высокой твердости, сформированного плазменной наплавкой в среде азота и высокотемпературным отпуском. *Известия вузов. Физика*. 2019;62(10(742)):106–111.
16. Cahn J.W., Hillig W.B., Sears G.W. The molecular mechanism of solidification. *Acta Metallurgica*. 1964;12(12):1421–1439. https://doi.org/10.1016/0001-6160(64)90130-0
17. Slyadnikov E.E., Turchanovskii I.Yu. The order parameter and kinetics of a nonequilibrium phase transition stimulated by the action of a volumetric heat source. *Izvestiya vuzov. Fizika*. 2016;59(9):125–133. (In Russ.).

    Слядников Е.Е., Турчановский И.Ю. Параметр порядка и кинетика неравновесного фазового перехода, стимулированного воздействием объемного теплового источника. *Известия вузов. Физика*. 2016;59(9):125–133.
18. Slyadnikov E.E., Khon Yu.A., Kaminskii P.P., Turchanovskii I.Yu. Kinetics of nonequilibrium melting of a macrosystem initiated by the action of a volumetric heat source on it. *Inzhenerno-fizicheskii zhurnal*. 2020;93(2):403–415. (In Russ.).

    Слядников Е.Е., Хон Ю.А., Каминский П.П., Турчановский И.Ю. Кинетика неравновесного плавления макросистемы, инициированного воздействием на нее объемного теплового источника. *Инженерно-физический журнал*. 2020;93(2):403-415.
19. Mirzade F.Kh. Wave instability of a molten metal layer formed by intense laser irradiation. *Technical Physics*. 2005;50(8):993–998. http://dx.doi.org/10.1134/1.2014528
20. Das K.S., Ward C.A. Surface thermal capacity and its effects on the boundary conditions at fluid-fluid interfaces. *Physical Review E*. 2007;75:065303. http://dx.doi.org/10.1103/PhysRevE.75.065303
21. Nevskii S., Sarychev V., Konovalov S., Granovskii A., Gromov V. Formation mechanism of micro- and nanocrystalline surface layers in titanium and aluminum alloys in electron beam irradiation. *Metals*. 2020;10(10):1399. https://doi.org/10.3390/met10101399
22. Nevskii S.A. The mechanism of formation of micro- and nanocrystalline surface layers of titanium and aluminum alloys during electron beam processing. *Fundamental'nye problemy sovremennogo materialovedeniya*. 2020;17(10):385–395.

    Невский С.А. Механизм образования микро- и нанокристаллических поверхностных слоев титановых и алюминиевых сплавов при электронно-пучковой обработке. *Фундаментальные проблемы современного материаловедения*. 2020;17(10):385–395.

Information about the Authors / Сведения об авторах

Sergei A. Nevskii, *Dr. Sci. (Eng.), Assist. Prof. of the Chair of Science named after V.M. Finkel',* Siberian State Industrial University
ORCID: 0000-0001-7032-9029
E-mail: nevskiy_sa@physics.sibsiu.ru

Сергей Андреевич Невский, *д.т.н., доцент кафедры естественно-научных дисциплин им. профессора В.М. Финкеля,* Сибирский государственный индустриальный университет
ORCID: 0000-0001-7032-9029
E-mail: nevskiy_sa@physics.sibsiu.ru

Lyudmila P. Bashchenko, *Cand. Sci. (Eng.), Assist. Prof. of the Chair "Thermal Power and Ecology",* Siberian State Industrial University
ORCID: 0000-0003-1878-909X
E-mail: luda.baschenko@gmail.com

Viktor E. Gromov, *Dr. Sci. (Phys.-Math.), Prof., Head of the Chair of Science named after V.M. Finkel',* Siberian State Industrial University
ORCID: 0000-0002-5147-5343
E-mail: gromov@physics.sibsiu.ru

Oleg A. Peregudov, *Cand. Sci. (Eng.), Vice-Rector for Youth Policy and Educational Activities,* Omsk State Technical University
ORCID: 0000-0001-5154-5498
E-mail: olegomgtu@mail.ru

Anastasia N. Gostevskaya, *Postgraduate of the Chair of Science named after V.M. Finkel',* Siberian State Industrial University
ORCID: 0000-0002-7328-5444
E-mail: lokon1296@mail.ru

Taras V. Volodin, *Head of the Department of Scientific Research,* Siberian State Industrial University
E-mail: volodin_tv@sibsiu.ru

Людмила Петровна Бащенко, *к.т.н., доцент кафедры теплоэнергетики и экологии,* Сибирский государственный индустриальный университет
ORCID: 0000-0003-1878-909X
E-mail: luda.baschenko@gmail.com

Виктор Евгеньевич Громов, *д.ф.-м.н., профессор, заведующий кафедрой естественнонаучных дисциплин им. профессора В.М. Финкеля,* Сибирский государственный индустриальный университет
ORCID: 0000-0002-5147-5343
E-mail: gromov@physics.sibsiu.ru

Олег Александрович Перегудов, *к.т.н., проректор по молодежной политике и воспитательной деятельности,* Омский государственный технический университет
ORCID: 0000-0001-5154-5498
E-mail: olegomgtu@mail.ru

Анастасия Николаевна Гостевская, *аспирант кафедры естественнонаучных дисциплин им. профессора В.М. Финкеля,* Сибирский государственный индустриальный университет
ORCID: 0000-0002-7328-5444
E-mail: lokon1296@mail.ru

Тарас Витальевич Володин, *начальник управления научных исследований,* Сибирский государственный индустриальный университет
E-mail: volodin_tv@sibsiu.ru

Contribution of the Authors / Вклад авторов

S. A. Nevskii – problem statement, obtaining and analyzing the dispersion equation, discussion and verification of modeling results.

L. P. Bashchenko – conducting calculations, discussion of the results, design of the article.
V. E. Gromov – analysis and discussion of the results of analysis of the structure of deposited high–speed steel by scanning electron microscopy.
O. A. Peregudov – discussion of the results, analysis of literary sources on the Mallins-Sekerki instability.
A. N. Gostevskaya – conducting research using scanning electron microscopy of deposited high-speed steel, discussion of the results.

T. V. Volodin – conducting research using scanning electron microscopy of deposited high-speed steel, discussion of the results.

С. А. Невский – постановка задачи, получение и анализ дисперсионного уравнения, обсуждение и верификация результатов моделирования.
Л. П. Бащенко – проведение расчетов, обсуждение результатов, оформление статьи.
В. Е. Громов – анализ и обсуждение результатов исследования структуры наплавленной быстрорежущей стали методами сканирующей электронной микроскопии.
О. А. Перегудов – обсуждение результатов, анализ литературных источников по неустойчивости Маллинза–Секерки.
А. Н. Гостевская – проведение исследований методами сканирующей электронной микроскопии наплавленной быстрорежущей стали, обсуждение результатов.
Т. В. Володин – проведение исследований методами сканирующей электронной микроскопии наплавленной быстрорежущей стали, обсуждение результатов.

Received 11.09.2023
Revised 25.09.2023
Accepted 18.12.2023

Поступила в редакцию 11.09.2023
После доработки 25.09.2023
Принята к публикации 18.12.2023